In situ Raman monitoring of studtite formation under alpha radiolysis in ^{18}O-labeled water

Aurélien Perrot, Aurélien Canizares, Sandrine Miro, Laurent Claparede, Renaud Podor, Thierry Sauvage, Sylvain Peuget, Christophe Jegou, Nicolas Dacheux

In situ Raman monitoring of studtite formation under alpha radiolysis in ^{18}O-labeled water

Aurélien Perrot[a], Aurélien Canizares[b], Sandrine Miro[a,*], Laurent Claparede[c], Renaud Podor[c], Thierry Sauvage[b], Sylvain Peuget[a], Christophe Jegou[a], Nicolas Dacheux[c]

[a] *CEA, DES, ISEC, DPME, Univ Montpellier, Marcoule, France*
[b] *CEMHTI, Univ d'Orléans, Orléans, France*
[c] *ICSM, Univ Montpellier, CNRS, CEA, ENSCM, Site de Marcoule, Bagnols/Cèze, France*
**sandrine.miro@cea.fr*

Abstract

Studtite $[(UO_2)(O_2)(H_2O)_2]\cdot 2(H_2O)$ is a secondary phase precipitating during the alteration of uranium-bearing materials. The mechanistic link between the formation of uranyl and peroxide bonds in the solid and the nature of the oxidizing species produced by water radiolysis remains to be elucidated. In order to improve our understanding of these mechanisms, an original experimental methodology in the presence of ^{18}O isotopes and Raman spectroscopy has been developed. It appears that there is a direct chemical relationship between the peroxo ligands inside studtite and the peroxide entities of H_2O_2 molecule into the solution. The link between H_2O_2 formation mechanism in solution by the radiolysis of water, the nature of the radiation and the isotopy of the peroxo ligands inside studtite has been described thanks to a coherent set of experimental data. For the uranyl UO_2^{2+} ions, the characterization of its isotopy allows to specify the mechanism of oxidation at the UO_2 /water interface. The isotopic configurations observed for the uranyl ion inside studtite, can be explained by assuming an oxidation mechanism of UO_2 involving both a simple transfer of electrons by interaction with H_2O_2 and the incorporation of oxygen atoms from the solution into the fluorite structure via OH° radicals.

Keywords: Nuclear fuel; Oxidative dissolution; Uranium dioxide; Irradiation; Hydrogen peroxide; Spectroscopy

1. Introduction

Water in interaction with heterogeneous nuclear materials such as spent fuel (UO_2 or $(U,Pu)O_2$ based ceramic), fuel debris or molten nuclear fuel (corium) produces hydrogen peroxide by radiolysis [1-4]. Interaction between the surface and hydrogen peroxide induces oxidative dissolution of uranium oxide and the precipitation of U(VI) secondary phases such as studtite $[(UO_2)(O_2)(H_2O)_2]\cdot 2(H_2O)$, a common uranium peroxide that generally forms under strongly oxidizing conditions. It has been the subject of important studies over the past 20 years as it can potentially incorporate radionuclides, play a protective role during spent fuel alteration or even control uranium solubility in solution [3-9]. Studtite has also been observed in natural deposits such as barite solid solutions incorporating ^{226}Ra and associated with other uranyl minerals such as rutherfordine or uranophane [10]. The crystallographic structure of this uranium peroxide is well known [11]. It is composed of ribbons of U-coordination polyhedra with shared edges, which are composed of O_2^{2-} bridging peroxo ligands.

There are also numerous studies on the stability of uranium peroxides as a function of solution chemistry, irradiation conditions and temperature [12-16]. For example, with regard to solution chemistry, the presence of carbonate ligand and H_2O_2 in groundwater increase studtite dissolution and uranium (U) release [12]. The stability under γ and α irradiation of studtite, and more generally of uranyl peroxide-based solid materials, with various structural topologies, has also been studied by XRD and Raman spectroscopy [13, 14]. Studtite is particularly affected by α irradiation which induces the formation of amorphous uranyl peroxide [14]. In addition, an increase in temperature leads to the loss of water molecules and the formation of metastudtite $(UO_2)(O_2)(H_2O)_2$, or even that of an amorphous compound [15, 16].

Despite of all these studies, the link between the radiolytic products of water (i.e. radicals and molecular species) and the formation of the uranyl ion and peroxo ligands within studtite needs to be better understood, requiring further investigation. Recently, a study coupling Raman spectroscopy with γ irradiation of ^{18}O labelled water has shown the possibility of linking the formation of radiolysis products to the main structural entities of studtite, namely peroxo ligands and uranyl ion [17]. The goal of the present work is to perform this study under α irradiation by monitoring studtite precipitation using in-situ Raman spectroscopy and ^{18}O labelled water irradiated by 5 MeV He^{2+} particles. This can be achieved using the in-situ irradiation Raman set-up implemented at the CEMHTI cyclotron beamline, which has already been used in previous studies [18, 19]. The originality of this work lies in the use of ^{18}O labelled water. Indeed, the gathering of Raman spectra coupled with solution analysis is expected to provide new insights to propose studtite formation mechanisms. The respective roles of hydrogen peroxide and radicals in the formation of peroxo and uranyl bonds will be particularly evaluated. The nature of isotopic exchanges under irradiation will provide a better understanding of the effects of Linear Energy Transfer (i.e. high or low LET effect) in studtite formation and, more broadly, in the mechanism of oxidative dissolution of uranium dioxide.

2. Materials and methods

2.1. Sample preparation

The target used for the alpha radiolysis experiment came from a sintered pellet of depleted UO_2, manufactured at CEA Cadarache, and was obtained after wire saw cutting and mirror polishing with diamond paste. The resulting UO_2 disk measured 8 mm in diameter and was 277 µm thick, stored in air within membrane storage boxes. Prior to leaching, three cycles of pre-leaching of the experimental device (cell and pellet) were carried out in a water solution (MilliQ Water) in the presence of 10^{-3} mol.L^{-1} $NaHCO_3$, in order to ensure the stoichiometry at the sample surface by removing the pre-oxidized surface layer. The pre-leaching steps lasted 1 hour, with the exception of the last one, which was extended to 14 hours. This pre-leaching was followed by three washing stages in the presence of the leaching cell, two washing stages were performed with pure water (MilliQ Water) and the last one was performed with ^{18}O-labelled water.
In order to carry out a complementary experiment to study the alteration of UO_2 without irradiation but in the presence of ^{18}O-labelled hydrogen peroxide, a second UO_2 sample was synthesized. This sample was prepared according to the process described by Martinez et al., i.e. by precipitating uranium (IV) in hydroxide form [20]. After washing, the precipitate obtained was deagglomerated then heated at 700°C for 4h under Ar/H_2 atmosphere. Finally, the powder was pelletized and sintered at 1550°C for 6h under Ar/H_2. The resulting sintered UO_2 pellet was fragmented. One of the fragments was annealed under Ar/H_2 atmosphere at 1100°C for 5h to ensure U/O stoichiometry. After synthesis and prior to leaching, the sample was characterized by Raman spectroscopy. It then underwent a 4 stages pre-leaching cycle in the presence of 10^{-3} mol.L^{-1} $NaHCO_3$. Pre-leaching lasted 1 hour, with the exception of the last one, which was extended for 12 hours. These steps were followed by two washing stages with deionized water and a last one with ^{18}O labelled water.

2.2. Leaching experiments

2.2.1. Leaching of UO_2 sample under α irradiation in presence of $H_2{}^{18}O$

Irradiation conditions. An external helium irradiation beam was used to irradiate the $UO_2/H_2{}^{18}O$ system. This irradiation was performed at the CEMHTI cyclotron, using 45 MeV $^4He^{2+}$ ions. The He^{2+} ion beam was collimated to obtain a 6 mm diameter centred on the UO_2 target. The 277 µm thickness of the UO_2 target was chosen according to the results of the SRIM software [21], which evaluated the trajectory and the dissipated energy of ions passing through a material. The SRIM-calculated energy of $^4He^{2+}$ ions at the UO_2 disk exit was 7.7 ± 0.9 MeV, with UO_2 density of 10.74 g.cm^{-3} (98 % theoretical density) and taking into account the presence of three 26.8 µm-thick titanium foils at the beam controller. Atom displacement energies have been set at 20 eV for oxygen and 40 eV for uranium, based on calculation of Soullard et al. [22]. The calculated projected range of these 7.7 MeV $^4He^{2+}$ ions, which induce water radiolysis in $H_2{}^{18}O$, was 71.8 ± 0.8 µm. The irradiation lasted 6 hours at an intensity of 10 nA, only during the first 35 minutes, then the intensity was decreased to 5 nA to limit the appearance of dihydrogen bubbles. The corresponding fluxes were 5.5×10^{10} α.cm^{-2}.s^{-1} for 5 nA and 1.1×10^{11} α.cm^{-2}.s^{-1} for 10 nA, to reach a final fluence of 1.3×10^{15} α.cm^{-2}. Based on fluence and SRIM simulation data [21], the displacement per atom (dpa) within the uranium dioxide layer probed by Raman spectroscopy (~1 µm) was calculated at 4.0×10^{-4} dpa. This value corresponds to a measure of the number of atoms ejected from their initial position in the crystal lattice, following ballistic collisions. It provides us a quantitative means of assessing the damage inflicted on the material by irradiation. However, it does not take into account defect recombination.

Experimental set-up in the irradiation chamber. This set-up allowing in-situ Raman monitoring of the $UO_2/H_2{}^{18}O$ interface during and after irradiation is presented in **Figure 1.** It consists of a leaching cell, manufactured in a polymer material resistant to radiolytic species attacks (PCTFE) in which the UO_2 target is placed and held in place by a system of screwed rings to ensure watertightness. The leaching

solution used was ^{18}O-enriched deionized water (97.17% ^{18}O, 0.34% ^{17}O, 2.49% ^{16}O, INNOVA-CHEM, France). During irradiation, the α beam is transmitted through the UO_2 specimen inducing water radiolysis. Finally, a 40 mm diameter quartz window located on the opposite side of the UO_2 sample provides optical access for in-situ Raman monitoring of the $UO_2/H_2{}^{18}O$ interface.

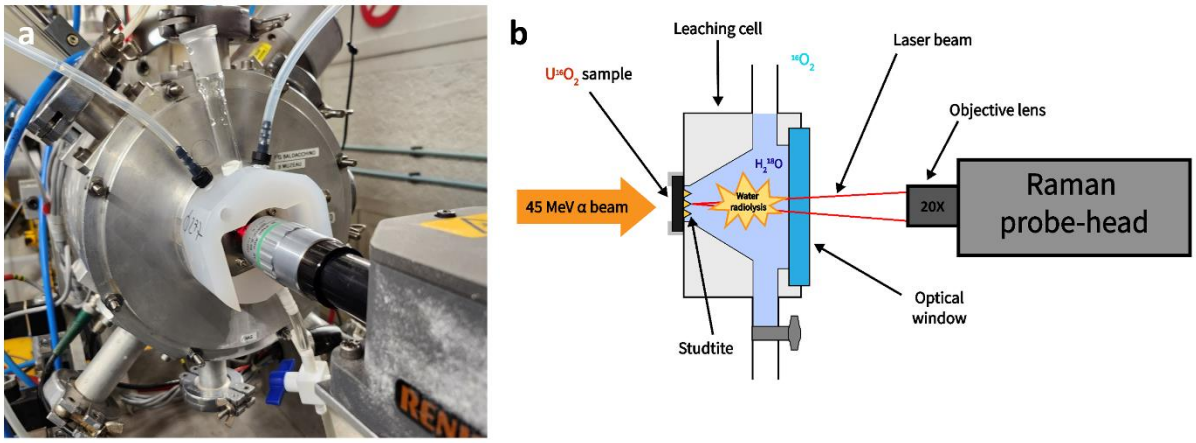

Figure 1. *In situ experimental set-up combining a leaching cell under α- irradiation with Raman monitoring: a. picture of the instrumental set-up; b. schematic diagram of the set-up, inspired from [18].*

In-situ Raman spectroscopy. Raman measurements were performed continuously on the direction parallel to the $^4He^{2+}$ beam direction (**Figure 1**), using a Renishaw RA100 spectrometer equipped with a He-Ne excitation laser (633 nm). The laser beam was delivered to the irradiation cell via a multimode optical fiber and a Renishaw's RP10 probe, equipped with a Mitutoyo long working distance (30.5 mm) objective which offers a 0.28 numerical aperture and with a 20x magnification. The 7 mW laser power measured at the sample surface allows a very good compromise between UO_2 disk laser damage resistance and Raman efficiency. The spectra were recorded with a 1800 groove/mm holographic grating, allowing 4 cm^{-1} spectral resolution and offering simultaneous observation from 310 to 1244 cm^{-1}, and an accumulation time of 2 minutes for each spectrum. Raman monitoring was carried out during a 21-hour leaching period, enabling the continuous observation of studtite precipitation, including post-irradiation precipitation induced by radiolytic products remaining in solution after a 6-hour irradiation period.

When the leaching test was stopped, the solution was drained, followed by 3 successive washes of the cell with pure water. The pellet was then taken off and carefully dabbed with Kimtex© paper to remove water and stop surface alteration, ensuring no rubbing occurred during the process.

2.2.2. Leaching of UO_2 in presence of $H_2{}^{18}O_2$

To understand the role of oxidizing species during water radiolysis, an additional leaching experiment was carried out by replacing the presence of these radiolytic species produced in ^{18}O-labelled water with a $H_2{}^{18}O_2$ solution. The 10^{-3} $mol.L^{-1}$ $H_2{}^{18}O_2$ solution was prepared from a commercial solution (Sigma-Aldrich Hydrogen Peroxide - $^{18}O_2$ Solution - 2-3% in H_2O, 90 atom % of ^{18}O) diluted with $H_2{}^{18}O$ water. The H_2O_2 concentration was verified in the resulting solution by the Ghormley method [23]. The sample was weighed and placed in a 10 mL leaching tube for 48 hours in the presence of 5 mL of 10^{-3} $mol.L^{-1}$ $H_2{}^{18}O_2$ solution. After leaching, the samples were characterized by Raman spectrometry, while the leachates were filtered to 3 kDa by centrifugation before being analysed by ICP - OES.

2.3. Post-mortem characterization

ESEM. ESEM (Environmental Scanning Electron Microscopy) characterization was carried out to observe the morphology of studtite precipitated on the pellet surface, using a ThermoFischer Scientific

Quattro S SEM. Micrographs were recorded using a voltage varying between 1 and 10 kV and a pressure in the chamber between 10^{-3} and 10^{-4} Pa.

Following an initial observation of the pellet's surface, an analysis of its cross-section was conducted. Prior to this second ESEM observation, the irradiated sample was vacuum-coated in resin, cut with a Buehler IsoMet 1000 milling cutter, then polished with a Buehler Beta polishing machine using diamond paste 1 µm to achieve a mirror-polished surface. To prevent charge accumulation onto the surface, the cross-section was coated with carbon prior to SEM observation.

X-Rays Diffraction. Structural analysis of the solids was carried out by X-ray diffraction (XRD) using a Bruker D8 ADVANCE diffractometer (Cu-Kα_1 radiation, λ =1.5406 Å, 40 kV, 40 mA, LinxEye detector). XRD patterns were collected at room temperature over the 5-100° (2θ) range, using a step size of 0.009° and a duration per step equal to 1 s.

ICP-OES/ICP-MS. Concentrations of uranium released in the leachate were first determined using a iCAP 7000 series optical plasma emission spectroscopy (ThermoFischer Scientific). The analysis was performed considering the results obtained at λ = 385.958 nm. In a second step, solutions with uranium concentrations below the limit of quantification by ICP-OES (LOQ (U) ~ 100 ppb) were analysed by ICP-MS (LOQ (U) ~ 50 ppt). The elemental concentrations of uranium was calculated as the average of three replicates. The instrument used was a ThermoFischer Scientific iCAP RQ. For all elemental analyses, a calibration curve was produced using a range of diluted samples prepared from a certified solution, framing the concentration range under consideration. All samples were diluted with 0.2 mol.L^{-1} HNO_3 prior to analysis, to limit uranium adsorption onto the walls of the vials.

Raman spectroscopy. Post-mortem µ-Raman analyses were carried out using the LabRam ARAMIS spectrometer (Horiba Jobin-Yvon) to study the alteration of UO_2 sample leached in $H_2{}^{18}O_2$ solution. The instrument is equipped with He-Ne excitation laser (632.8 nm) and a Nd:YAG laser (532 nm). The laser beam was focused onto the sample surface using an Olympus BX 41 microscope equipped with a 100× SLMP objective. The resulting spot size was of the order of 1 μm^2. During spectra acquisitions, the laser (532 nm) was filtered down to 0.3 mW (measured at the sample surface) to avoid any sample modification. The spectra were recorded using the 1800 grooves.mm^{-1} holographic grating and taking into account accumulation time of 4 minutes per spectrum. These parameters were chosen to ensure a good signal-to-noise ratio. For the sake of reproducibility, different remote areas were analysed to confirm the homogeneity of the sample surface. Once the spectra have been recorded, they were processed using OriginPro (Version 2023b. OriginLab Corporation, Northampton, MA, USA) software. A baseline correction was performed and the spectra were then normalized to the band of maximum intensity.

3. Results

3.1. In-situ Raman monitoring of studtite precipitation under alpha irradiation

Uranium dioxide presents a fluorite-type crystal structure (CaF_2), characterized by a space group $Fm\bar{3}m$ (O_h^5). In this structure, the U^{4+} cations adopt a face-centred cubic (f.c.c.) arrangement, while the anions (O^{2-}) occupy the tetrahedral positions [24]. In accordance with group theory, a triply degenerate Raman-active vibrational mode at 445 cm^{-1} is observed in the initial Raman spectrum. This band, called T_{2g}, results from the antiphase oscillation of stretching oxygen atoms around uranium [25]. The initial spectrum admits other bands, including defect bands between 500 and 700 cm^{-1} (**Figure 2**). A broad band is also observed at 1150 cm^{-1}. This band has been assigned to a second-order longitudinal optic phonon (2LO) [24]. Finally, a band at 911 cm^{-1} was also identified, generally attributed to the $2TO_R$ mode [24, 26]. All spectra recorded during the leaching test were normalized in intensity with T_{2g} and then used to acquire a temporal Raman map (**Figure 2**). During the first few minutes of irradiation, dihydrogen was produced by radiolysis of water within the cell. This led us to make short interruptions of the irradiation at 10 nA to evacuate the bubbles present and to lower the beam intensity. During these stops, the recording of Raman spectra were stopped. These stops correspond to the grey lines observed in **Figure 2**.

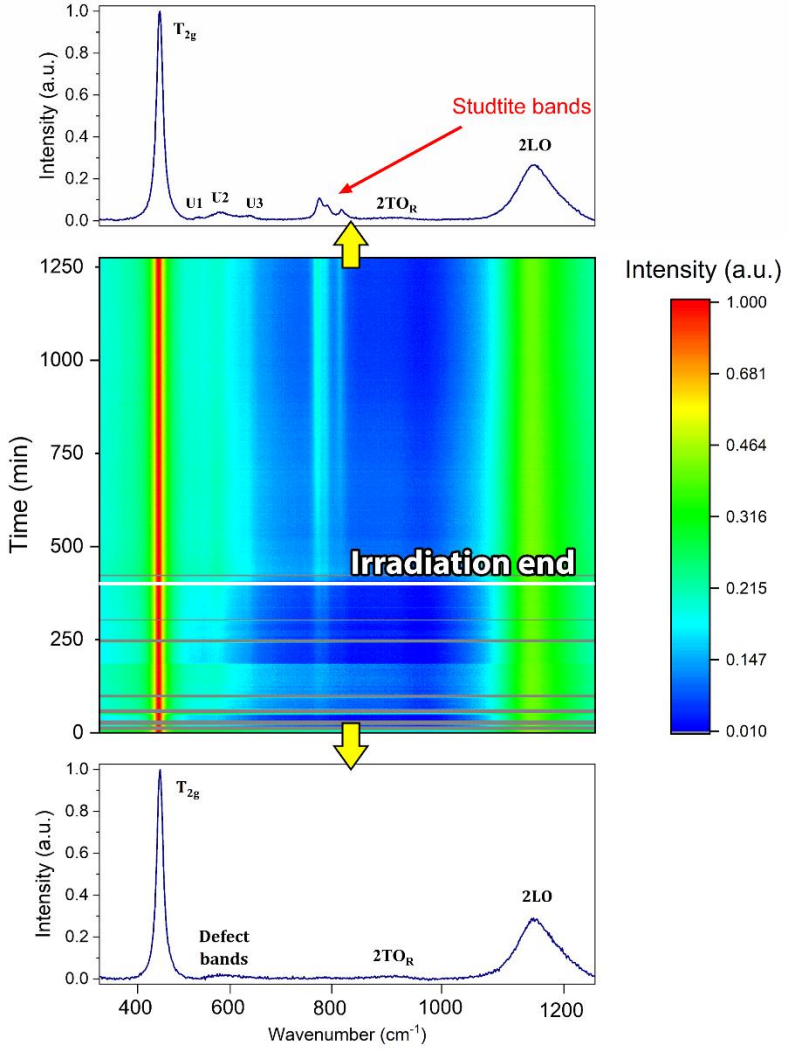

Figure 2. *2D time-resolved Raman spectra alteration with the pristine UO_2 signal (bottom) and the final spectrum showing studtite precipitation (top).*

The characteristic bands of the UO_2 compound were observed in all the Raman spectra recorded during the entire experiment. The final spectrum was still composed of the UO_2 fingerprint, in which no position and FWHM variation was detected in the T_{2g} and 2LO bands compared to the initial spectrum. No significant evolution of the FWHM was also observed by Gutierrez et al. for a dpa lower than 0.03 [27]. However, a significant evolution of the band associated with defects was observed between 500 and 700 cm^{-1}. The intensity of this defect band composed of three contributions: U_1, U_2 and U_3 is reported in **Figure 3a**. The increasingly pronounced appearance of these three defect bands during irradiation is clearly evidenced. Their growth was due to the ballistic impact of the He^{2+} ions in the fluorite structure. The latter is composed of 3 defect bands: Firstly, the U_1 band is present at 530 cm^{-1}, which assignment is still discussed [18, 28]. Indeed, it is sometimes associated with the distortion of the cubic lattice by interstitial oxygen. Secondly, the U_2 band at 577 cm^{-1}, which is assigned to the first-order longitudinal optical phonon (1LO) mode, active in IR and observable in Raman in the presence of defects in the fluorine structure, due to loss of symmetry. This loss of symmetry resulted from the appearance of oxygen clusters and the change in ionic radius between U (IV) and U (V) during oxidation [29, 30]. Lastly, the U_3 band at 634 cm^{-1} which is characteristic of the presence of oxygen cuboctahedra, is observed [28, 29, 31]. When irradiation was stopped, the increase of bands intensity stopped and the phenomenon was not reversible. No saturation appeared to have been reached before the end of irradiation. This observation is in good agreement with the results obtained by G. Guimbretière et al. Indeed, saturation was not yet observed for fluence values of 1.3×10^{15} $\alpha.cm^{-2}$ [32]. The displacement per atom (dpa) previously calculated tells us that alpha particles are transmitted with a very low impact on UO_2, revealing the extreme sensitivity of defect bands to irradiation-induced damages. In addition, in **Figure 2**, the growth of 3 bands at 774, 790 and 817 cm^{-1} can be noted. These bands correspond to the $[(UO_2)(O_2)(H_2O)_2]\cdot 2(H_2O)$ studtite compound and were already detected on ^{18}O labelled studtite [11, 17]. The observation of this phase under our conditions is consistent with the results obtained by Corbel et al. [33]. The intensity of the studtite characteristic bands is plotted against time in **Figure 3b**. The increase in their intensity clearly shows the formation of this phase from the very beginning of the experiment, and its subsequent growth during the experiment. The evolution of the Raman response of this phase allowed us to establish that studtite precipitation occurred according to a linear kinetic. It was observed that the linear evolution of the Raman response continues while the pellet is no longer irradiated, until around 1000 minutes. This result is in good agreement with the observations by R. Mohun who has reported that studtite kept growing despite the stop of irradiation [34]. After 1000 minutes dissolution experiment, precipitation slowed down.

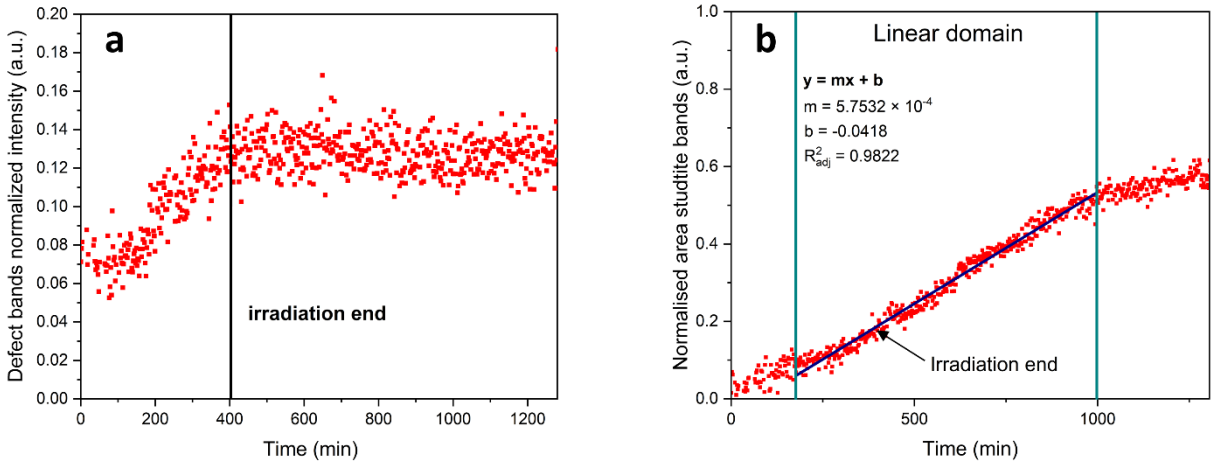

Figure 3. *Monitoring the time-dependent Raman response of bands normalized with T_{2g} during the leaching time. Evolution of the area of defect bands (a) and evolution of band area associated with studtite (b).*

3.2. Analysis of the solutions and post-mortem characterization of the studtite layer

The study of UO_2 alteration by water radiolysis is well documented in the literature [4, 17, 33, 35]. Consequently, studtite precipitation under these experimental conditions can be anticipated and should occur as soon as saturation of this phase in solution is reached. To correlate uranium release with studtite precipitation, the concentration of uranium in solution during the leaching test was measured. First, the pre-leaching steps ensured that the oxidized surface layer of the UO_2 pellet was removed. Thus, the effectiveness of the washing steps carried out after this pre-leaching stage was monitored, verifying that all the uranium present in the leach cell was recovered. This then enabled a balance to be drawn up for the uranium in solution. For all these reasons, the uranium concentration was determined after each stage (**Table 1**).

A low concentration of uranium released during the pre-leaching stage was noted, indicating a weak pre-existing oxidized layer of U(VI). This observation seems to be in agreement with the initial Raman response of the pellet, which did not show significant defect bands (in particular the U_3 band).

After the leaching test, the uranium concentration of the leaching solution was measured at $(1.1 \pm 0.1) \times 10^{-4}$ mol.L^{-1}, from which a quantity of uranium released into solution equal to $(5.9 \pm 0.5) \times 10^{-7}$ mol was deduced. These release values are in agreement with the release previously obtained by Corbel et al. [33].

A speciation calculation was carried out using CHESS software [36] and the ThermoChimie database [37]. At the end of the leaching stage, the saturation index in uranium was determined to be 2.58 at a pH of 3. This value confirms that the conditions in the solution were oversaturated with respect to studtite during leaching, resulting in the precipitation of this phase.

The thickness of the studtite layer was estimated using the data reported by Corbel et al. under similar conditions [33]. Knowing the output energy of the alpha particles (7.7 MeV) and the fluence at the end of the experiment (1.3×10^{15} α.cm^{-2}), it can be calculated that the total energy deposited in the solution is 456 J. Corbel et al. have established a relationship between this deposited energy and H_2O_2 concentration, allowing us to estimate that the H_2O_2 concentration present at the end of irradiation was $C_{H_2O_2} \approx 6 \times 10^{-3}\ \mathrm{mol \cdot L^{-1}}$ [33]. From the H_2O_2 concentration and a second relationship established by Corbel et al, a layer growth rate of 100 nm.h^{-1} was able to be estimated, enabling the determination of the precipitated studtite layer's thickness at 2.1 µm. With the knowledge of studtite's density (3.64 g.cm^{-3}) [38], it can be deduced that the mass of studtite that was precipitated on the pellet's surface amounts was approximately 1 mg.

Table 1. *Uranium concentration determination in solution during pre-leaching, washing and leaching stages when leaching UO_2 irradiated with α particles*

Sample	Duration (h)	Solution	Volume (mL)	C_U (mol.L^{-1})
Pre-leaching 1	1	$NaHCO_3$	4.5 ± 0.1	**$(1.7 \pm 0.1) \times 10^{-7}$**
Pre-leaching 2	1			**$(1.5 \pm 0.1) \times 10^{-8}$**
Pre-leaching 3	14			**$(1.8 \pm 0.1) \times 10^{-9}$**
Washing 1	--	H_2O	4.5 ± 0.1	**$(1.6 \pm 0.1) \times 10^{-8}$**
Washing 2	--			**$(2.0 \pm 0.3) \times 10^{-10}$**
Washing 3	--	$H_2{}^{18}O$	12.5 ± 0.2	**$(2.5 \pm 0.1) \times 10^{-9}$**
Leaching	21	$H_2{}^{18}O + \alpha^*$	5.5 ± 0.1	**$(1.1 \pm 0.1) \times 10^{-4}$**

**6 hours of irradiation*

Once the radiolysis experiment was completed, the UO_2 disk was first characterized by X-ray diffraction (XRD) to identify crystal phases. The X-ray pattern obtained (**Figure 4**) in reflectivity mode with normal incidence, revealed the coexistence of two different phases: UO_2 and studtite

$[(UO_2)(O_2)(H_2O)_2]\cdot 2(H_2O)$. This compound crystallizes in a monoclinic structure with space group C2/c [11].

The recorded diffractogram is compared with the studtite diffractogram reported by Burns et al. [11]. Thus, the XRD diffractogram revealed a strong anisotropy in the intensity of the lines, marked by a crystal growth surface favoured along the (-202) plane, associated with a position of 21.12° (2θ). The ratio of peak amplitudes (1,1,0)/(-2,0,2) is ~5.34, whereas it is ~0.13 for our sample [11]. Thus, it can be deduced, as shown in **Figure 4**, that studtite chains are oriented parallel to the axis of needle growth, this axis corresponding to the c-axis. The orientation of studtite within a needle is illustrated in **Figure 4a**, where the (-202) plane (**Figure 4b**) is arranged perpendicular to the growth direction while the (200) plane (**Figure 4c**) is aligned parallel along the growth axis. The work of Corbel et al. did not identify any preferential orientation in the formation of studtite under alpha irradiation [33], however, our results are consistent with the observations of Schlegel and Jegou who reported the presence of a preferential orientation of crystal growth along (-202) in the case of precipitation without irradiation [39]. Two hypotheses may be put forward to explain this contradiction. On the one hand, if irradiation does indeed inhibit studtite formation with preferentially oriented textures, our finding could result from the fact that, in our experiments, studtite growth mainly occurred in the absence of irradiation, during the last part of the experiment, when the beam was off. This could lead to a diffractogram that is predominantly representative of studtite that grew without the influence of irradiation. On the other hand, it's important to point out that studtite growth duration reported by Corbel et al. was significantly shorter than that observed in our study, with a maximum of 6h for continuous irradiation. However, research by Schlegel and Jegou has shown that the orientation effect along the (-202) plane is only perceptible after six hours of precipitation [39]. This time difference could therefore play a crucial role in whether or not orientation effects are observed, providing a second hypothesis to explain the observed contradiction.

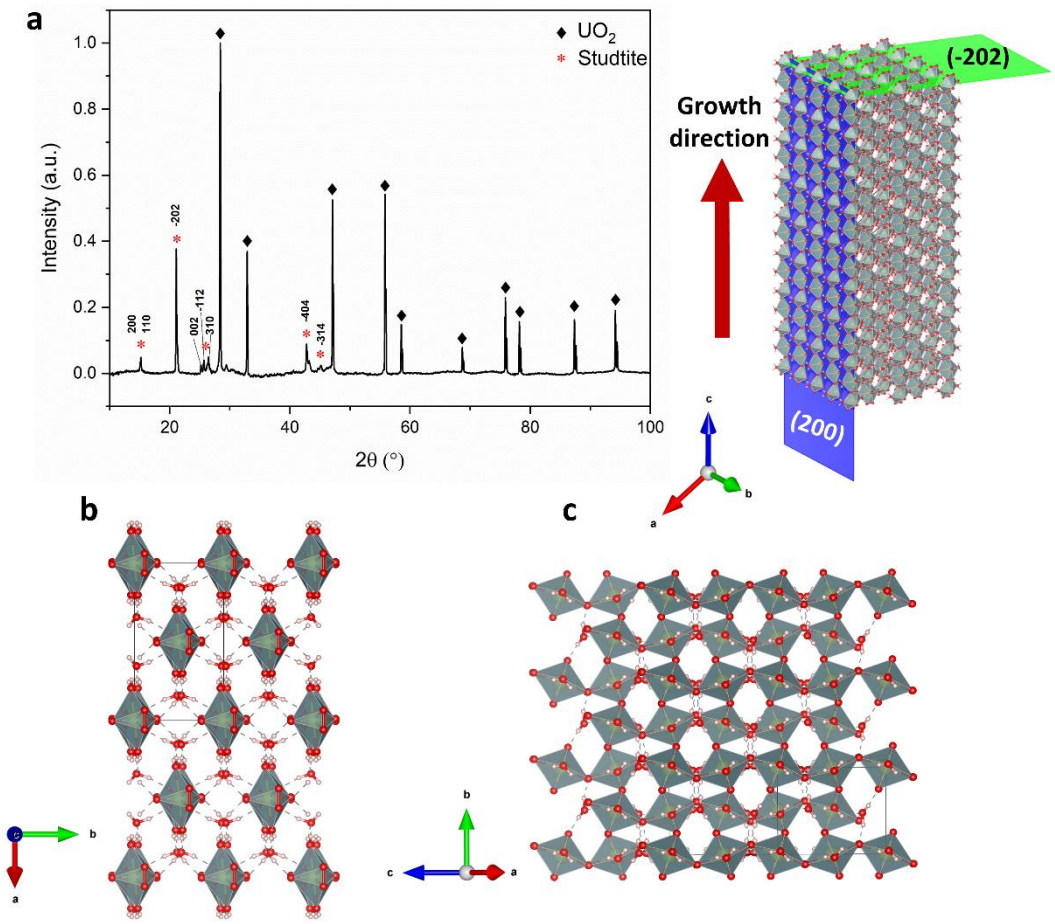

Figure 4. *XRD diagram and structural analysis of studtite growth: a. XRD pattern of UO_2 pellet after leaching, showing the formation of studtite at the solid/solution interface (left) and schematic illustration of the structure of studtite during crystal growth (right); uranium atoms being at the center of the coordination polyhedra; b. View of the plans (−202) and (−404); c. View of the plan (200)*

ESEM observations of the UO_2 disk reported in **Figure 5**, confirmed the formation of a homogeneous crystalline layer characteristic of the studtite phase formed during the oxidative dissolution of UO_2 in presence of H_2O_2 [33]. The area that was not in contact with the solution (**Figure 5a**) does not show any secondary phase or alteration marks on the surface. Only marks due to the polishing process such as scratches and grain tears are observed, whereas a layer covered with needle-like studtite crystals was formed on the area in contact with the solution (**Figure 5b**).

In addition, the observation of the cross-section of the pellet (**Figure 5c**) allowed us to image the alteration layer and to determine the morphology of the crystal growth. A single homogeneous layer of studtite, formed by needles grown perpendicularly to the UO_2 surface, with an average height of about 1.4 µm, was observed. The studtite thickness measured is in accordance with that which has been previously estimated by leachate analysis (i.e. 2.1 µm).

The SEM observations of the studtite layer clearly indicate that the needles have grown according to a preferential orientation. This result is in good accordance with XRD data, where a texture marked by preferential orientation of crystal growth was observed (**Figure 4**).

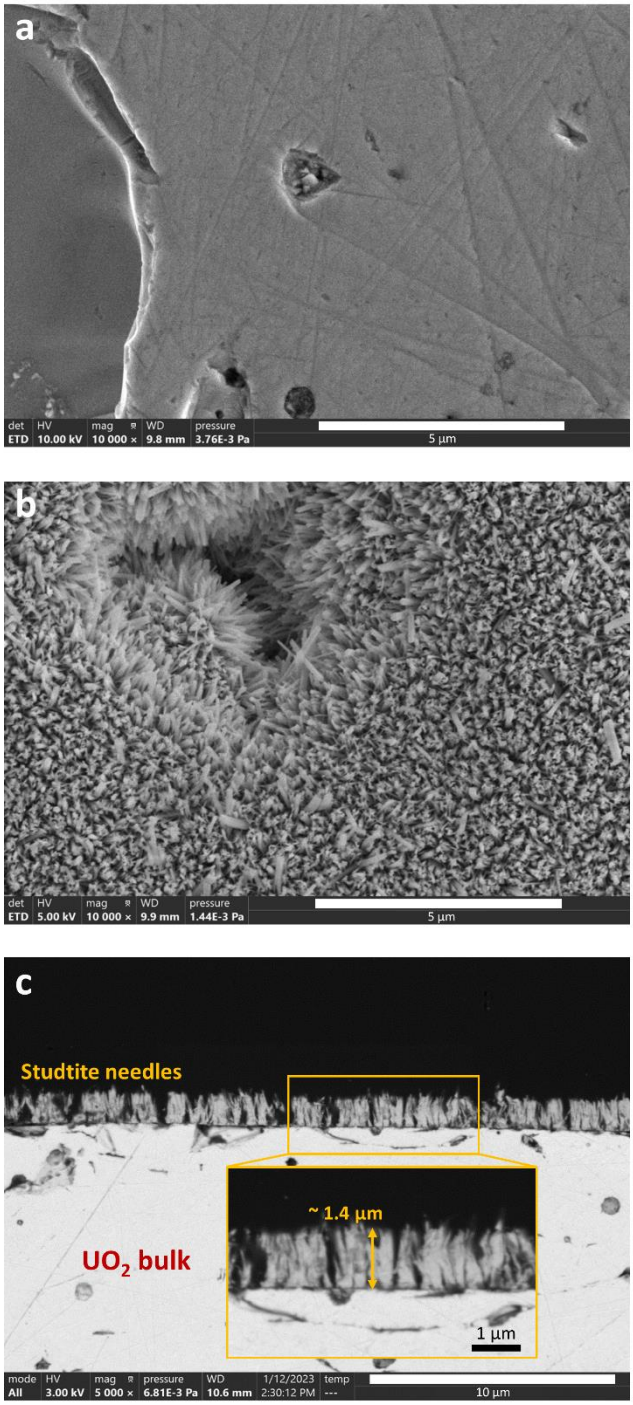

Figure 5. ESEM micrographs of UO_2 leached pellet: a. Non-leached peripheral zone; b. Altered surface covered with a layer of studtite needle-like crystals; c. Cross-section of the pellet.

3.3. Analysis of studtite isotopic enrichment

The use of ^{18}O enriched water and Raman spectroscopy offer a precise method to determine the origin of the oxygen present in studtite and to deduce its formation mechanisms. In order to analyse the enrichment of the different bonds in studtite, it was first necessary to determine the different Raman band positions of ^{18}O enriched studtite. To evaluate the theoretical vibration frequencies and deduce the wavenumber associated with each ^{18}O enriched studtite bond, it was considered that an

intramolecular stretching vibration can be described by a harmonic oscillator model in which the binding force is described by the Hooke's law [40].

$$\tilde{\nu} = \frac{1}{2\,\pi c}\sqrt{\frac{k}{\mu}} \quad (1)$$

where $\tilde{\nu}$ is the wavenumber (in cm^{-1}), c is the speed of light (in $cm.s^{-1}$), k is the binding force constant (in $kg.s^{-2}$) and μ corresponds to the reduced mass (in kg). There is a direct relationship between mass and bond vibration frequency. Isotopic labelling thus induces a shift in the Raman bands by modifying the mass of the original atoms. To determine the position of the bands after isotopic enrichment, the experimental position of the isotopically unlabelled bands was used and then the calculated shift was applied [17].

In the case of studtite, its response to isotopic labelling is characterized by a behaviour similar to that of a free molecule, where each possible isotopic configuration is associated with a specific Raman response. This is in contrast to solids, which generally show a single band per bond, integrating the different contributions [17]. The calculated vibration frequencies associated with each of the different oxygen configurations within the peroxide and uranyl bonds of studtite are presented in **Table 2**.

Table 2. *Calculated Raman band positions associated with the contribution of the various bonds for O^{18} enriched H_2O_2, studtite and UO_2^{2+}*

Bond	Compound	Configuration	Experimental position (cm^{-1}) [17]	Calculated Raman band position for ^{18}O enriched compound (cm^{-1})
Peroxyde	H_2O_2	^{16}O-^{16}O	*876 (1)*	
		^{16}O-^{18}O		*851*
		^{18}O-^{18}O		*826*
	Studtite	^{16}O-^{16}O	*863 (1)*	
		^{16}O-^{18}O		*838*
		^{18}O-^{18}O		*814*
Uranyl	UO_2^{2+}	$^{16}O = U = {}^{16}O$	*870 (3)*	
		$^{16}O = U = {}^{18}O$		*845*
		$^{18}O = U = {}^{18}O$		*820*
	Studtite	$^{16}O = U = {}^{16}O$	*817 (2)*	
		$^{16}O = U = {}^{18}O$		*793*
		$^{18}O = U = {}^{18}O$		*770*

Figure 6 shows the Raman spectra of studtite from three leaching experiments together with the reference spectrum of studtite. Pseudo-Voigt function fits of the Raman spectra presented in **Figure 6** were performed on the bands present between 700 and 900 cm^{-1} associated with studtite, in order to assign the corresponding bonds to each band (**Table 2**) and thus deduce the isotopic enrichment of studtite.

As mentioned above, the Raman spectrum of pellet subjected to leaching by alpha irradiated labelled water shows a cluster of 3 bands between 700 and 900 cm^{-1} (**Figure 6a**). The first band at 774 cm^{-1} is

associated with the uranyl bond composed of two ^{18}O oxygen ($^{18}O = U = {}^{18}O$). The second band at 790 cm^{-1} is associated with the uranyl bond composed of one ^{18}O and one ^{16}O ($^{16}O = U = {}^{18}O$). Finally, the third band at 817 cm^{-1} is attributed to the sum of the contributions of the uranyl bond composed of two ^{16}O oxygen ($^{16}O = U = {}^{16}O$) and the peroxide bond composed of two ^{18}O oxygen ($^{18}O - {}^{18}O$). No bands at 840 cm^{-1} and 860 cm^{-1} attributed respectively to the peroxide bond ^{18}O - ^{16}O and ^{16}O - ^{16}O were observed despite the presence of ^{16}O (3 atom %) present in water.

For the stoichiometric UO_2 pellet submitted to a leaching by a 1mM $H_2{}^{18}O_2$ + $H_2{}^{18}O$ solution (**Figure 6b**), the Raman spectrum showed a band at 772 cm^{-1}, corresponding to the uranyl $^{18}O = U = {}^{18}O$ bond. A second band was seen at 788 cm^{-1}, corresponding to the uranyl $^{16}O = U = {}^{18}O$ bond. Finally, a last band located at 811 cm^{-1} was associated with the contribution of the uranyl $^{16}O = U = {}^{16}O$ bond, but also with that of the peroxide $^{18}O - {}^{18}O$ bond. A slight band at 860 cm^{-1} attributed to the peroxide ^{16}O - ^{16}O bond seemed to be present. This band is confused with the noise and the $2TO_R$ band at 925 cm^{-1} and was expected in these proportions due to the presence of ^{16}O (10 atom% ^{16}O) in the $H_2{}^{18}O_2$ enrichment. Sarrasin had noted for a pellet having undergone leaching by a gamma-irradiated labelled water (**Figure 6c**) the presence of a significant band associated with the ^{16}O - ^{16}O peroxide bond while the band at 817 cm^{-1} was weak [17]. Finally, the reference spectrum of studtite without isotopic labelling (**Figure 6d**) showed two bands at 817 cm^{-1} and 860 cm^{-1} corresponding to the uranyl ($^{16}O = U = {}^{16}O$) bond and the peroxide (^{16}O - ^{16}O) bond, respectively.

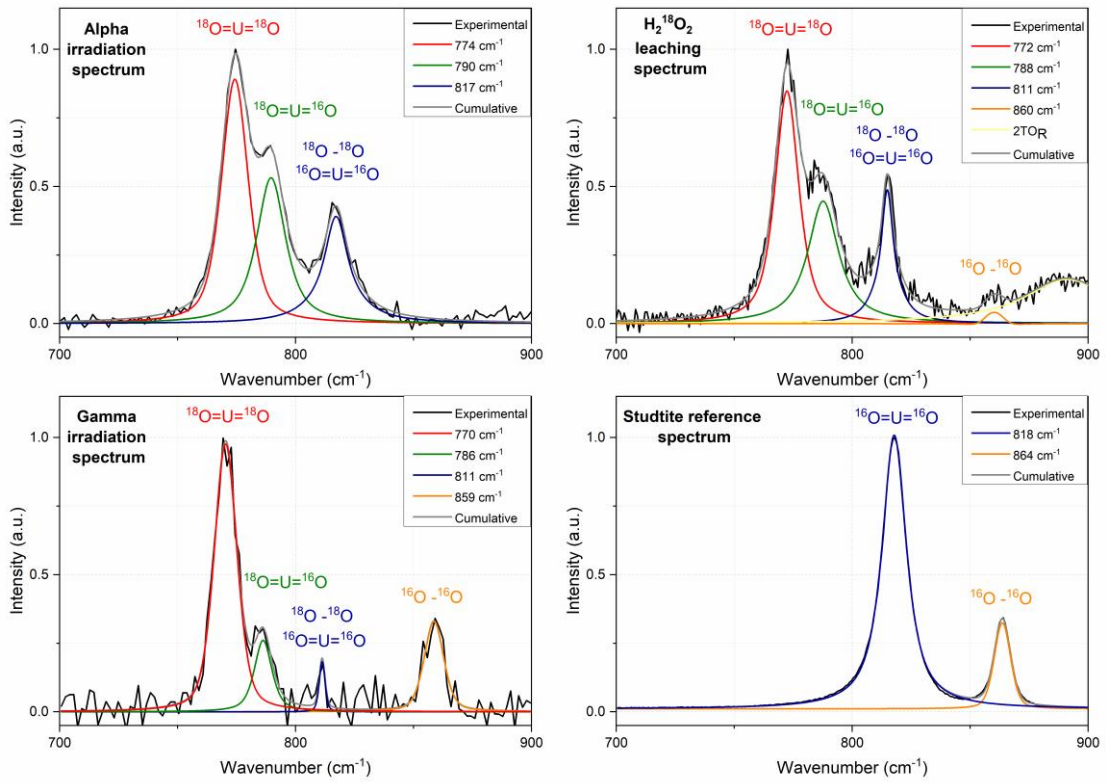

Figure 6. *Results of deconvolution of studtite Raman spectra recorded for UO_2 after 1 day of α radiolysis (a), UO_2 after 2 days of leaching with $H_2{}^{18}O_2$ (b) UO_2 after 1 day of γ radiolysis, based on the results of [17] (c) and studtite without any isotopic labeling (d)*

In order to quantify the isotopic proportion of each band, the method proposed by Sarrasin was carried out [17], which results are presented **Figure 7**. The model proposed by Sarrasin is a binomial distribution in which x corresponds to the isotopic abundance of ^{16}O while $1 - x$ corresponds to the isotopic abundance of ^{18}O. Thus, for the uranyl bond, the respective probabilities of the different

configurations are as follows: x^2 for $^{16}O=U=^{16}O$, $2x(1-x)$ for $^{16}O=U=^{18}O$ and $(1-x)^2$ for $^{18}O=U=^{18}O$. The intensity of the three uranyl peaks is directly proportional to the probability of a given isotopic configuration. By knowing the probabilities of the configurations, the isotopic abundance can be determined from the intensity ratios of the uranyl bands. Applying this model at the end of the leaching test of the UO_2 sample under α irradiation in $H_2{}^{18}O$, an isotopic fraction of 79% ^{18}O in the uranyl bond and 97% ^{18}O in the peroxide bond was obtained. Refinement of the recorded spectrum of studtite precipitated on stoichiometric UO_2 in the presence of $H_2{}^{18}O_2$, gave an isotopic fraction of 85% ^{18}O in the uranyl bond and 97% ^{18}O in the peroxide bond. No ^{16}O - ^{18}O band was found at 840 cm^{-1}. For these experiments, the process of studtite formation seems to have produced only oxygen groups of identical isotopy, and this feature has persisted over time.

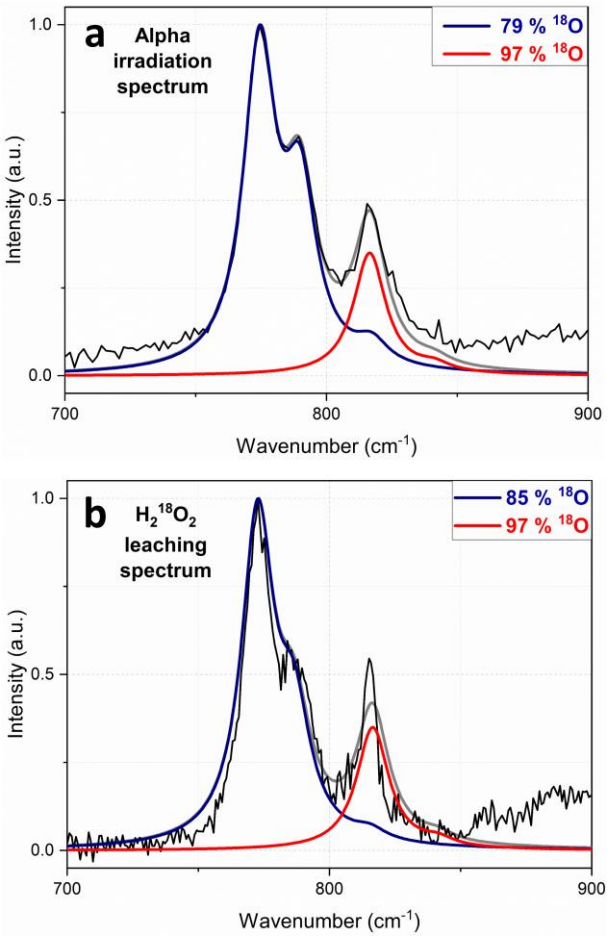

Figure 7. *Isotopic labeling fit of studtite bands by lorentzian function: a. UOx after 1 day with α radiolysis; b. UO_2 after 2 days of leaching with $H_2{}^{18}O_2$. The isotopic enrichment of uranyl (blue) and peroxide (red) bonds is shown on each graph.*

During leaching, a significant change in the isotopic ratio of the uranyl bond was observed, as shown in **Figure 8**. During irradiation, a band corresponding to $^{18}O=U=^{16}O$ was observed, with an intensity comparable to that of the band associated with the $^{18}O=U=^{18}O$ bond (**Figure 8a**). When irradiation was stopped, a change in the isotopic response occurred: the $^{18}O=U=^{16}O$ band became progressively weaker compared to that of the $^{18}O=U=^{18}O$ band (**Figure 8b**). The observation of an isotopic change when the beam is stopped suggests an evolution in studtite formation mechanism, with or without irradiation, which will be discussed later. The shape of the curve showing a gradual isotopic transition following the end of the irradiation can be attributed to the fact that the studtite layer as a whole influences the Raman response. As a result, the isotopic impact of studtite formed under irradiation remains despite the beam being stopped. The result is a direct link between the curve profile and the

kinetics of studtite growth after the beam is stopped (**Figure 3b**). Thus, the inflexion observed in the curve after 1000 minutes can either be interpreted as the attainment of a spectrum characteristic of studtite formed without irradiation, or as the result of a slowdown in precipitation.

Finally, it was not possible to obtain a satisfactory fit with the binomial distribution model, suggesting the existence of a mechanism for the formation of the specific uranyl bond during alpha irradiation. This mechanism seems to favour the formation of the $^{18}O{=}U{=}^{16}O$ bond during irradiation. The peroxide bond, on the other hand, is not affected by these changes during leaching.

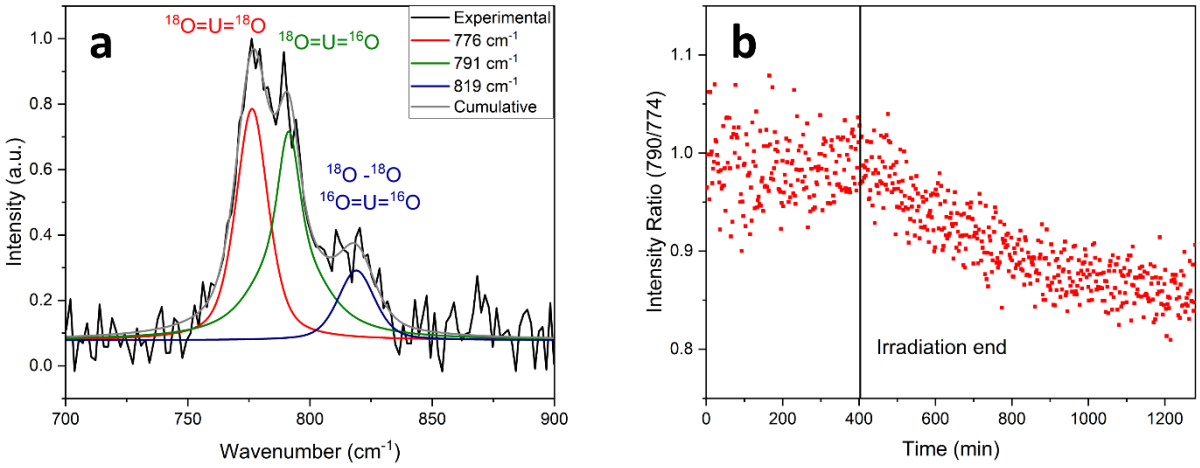

Figure 8. *Evolution of uranyl bond isotopy during leaching experiment a. spectrum recorded at the end of irradiation; b. intensity ratio of 790 cm^{-1} ($^{18}O{=}U{=}^{16}O$) to 774 cm^{-1} ($^{18}O{=}U{=}^{18}O$) bands.*

4. Discussion

In light of the results obtained, the first open question is to understand the chemical relationship between the peroxide bond of the H_2O_2 radiolytic product and the bridging peroxo ligand inside studtite.

Firstly, the reference leaching experiment of the UO_2 pellet in the presence of $H_2{}^{18}O_2$ shows that there is isotope exchange with the solution and secondly that the isotopy of the bridging peroxo ligand in studtite is directly linked to that of H_2O_2 in solution. Indeed, **Figure 7b** shows that in the presence of $H_2{}^{18}O_2$, the bridging peroxo ligand in studtite is predominantly ^{18}O-^{18}O. In other words, the stability of the peroxo ion is important and the peroxide bond is not broken when studtite precipitation occurs. Based on this observation, it is interesting to discuss the isotopy of the peroxide bond in studtite in relation to the radiolytic processes leading to the formation of H_2O_2 in solution under high and low LET radiation. **Figure 6** clearly shows that under alpha irradiation (high LET) the peroxide bond is predominantly ^{18}O-^{18}O, whereas it is mainly ^{16}O-^{16}O under gamma irradiation (low LET). Under water radiolysis, primary hydrogen peroxide is produced mainly by recombination of OH° radicals during the heterogeneous chemistry step (< 10^{-6} s) in the spurs generated by the energy deposition of alpha particles and gamma rays. However, under gamma irradiation, over longer periods and during the homogeneous chemistry stage (> 10^{-6} s), dissolved oxygen ($^{16}O_2$) in solution controls the final H_2O_2 concentration at steady state and is strongly involved in its formation processes [41-45]. Under gamma irradiation, dissolved oxygen leads to the formation of $H_2{}^{16}O_2$ by scavenging the H° radical and the aqueous electron according to the following reaction scheme:

$$H° + {}^{16}O_2 \rightarrow H{}^{16}O_2{}^{\circ} \quad (2)$$

$$e^-_{aq} + {}^{16}O_2 \rightarrow {}^{16}O_2{}^{\circ -} \quad (3)$$

$$H{}^{16}O_2{}^{\circ} + {}^{16}O_2{}^{\circ -} (+H_2O) \rightarrow \mathbf{H_2{}^{16}O_2} + {}^{16}O_2 + OH^- \quad (4)$$

$$H{}^{16}O_2{}^{\circ} + H{}^{16}O_2{}^{\circ} \rightarrow \mathbf{H_2{}^{16}O_2} + {}^{16}O_2 \quad (5)$$

This process, related to the presence of dissolved oxygen, has been the subject of several comparisons between radiolysis calculations and experimental measurements and is now well known and reported in the literature [41-45]. Under alpha irradiation, the primary production of H° radicals and aqueous electron is much lower than under gamma irradiation, therefore the production of H_2O_2 is not very sensitive to the presence of dissolved oxygen in the homogeneous solution. The main process of H_2O_2 formation in $H_2{}^{18}O$ labelled water remains the recombination of two $^{18}OH°$ radicals according to:

$$^{18}OH° + {}^{18}OH° \rightarrow \mathbf{H_2{}^{18}O_2} \quad (6)$$

The isotopic signatures of the peroxo ligands in studtite for the experiments carried out under alpha and gamma irradiation are therefore fully consistent with the formation processes of hydrogen peroxide in solution. A ^{16}O-^{16}O chemical bond is observed under gamma irradiation, whereas an ^{18}O-^{18}O bond is favoured under alpha irradiation. The presence of a peroxo ^{18}O-^{18}O bond under alpha irradiation also confirms the stability of water with respect to isotopic exchange over the duration of the experiment, which is consistent with the long-term studies conducted by Bonales [46].

The second objective is to obtain some information on the oxidative dissolution mechanism from the use of isotopes. For the uranyl bond, the isotopic composition of the oxygen atoms inside $UO_2{}^{2+}$ ions can provide information on the oxidative dissolution mechanisms of uranium dioxide. However, in order to ensure that the actinyl species keeps the memory of the dissolution mechanism, the residence

time of the oxygen atoms on the UO_2^{2+} ions must be long enough since its release from the surface to the studtite to be analysed by Raman spectroscopy. The isotopic exchange of oxygen atoms within the uranyl ion has been studied since the early 1960's. These studies [47, 48] have shown that the uranyl ion does not exchange its oxygen atoms with the solution for a period of 2000 hours, much longer than the duration of the experiments presented in this work. Similarly, studies of the nature of isotopic exchange between studtite and ^{18}O-enriched water have shown the absence of exchange with the peroxo and uranyl bonds within studtite [47]. These bonds are strongs and not very sensitive to isotopic exchange. The only fast exchanges are with the water molecules of studtite. Therefore, it is reasonable to assume that the oxygen isotope of the uranyl ion provides relevant information about the nature of the oxidative dissolution mechanism at the UO_2 / water interface.

The reference leaching experiment of the UO_2 pellet in the presence of $H_2{}^{18}O_2$ clearly shows that the uranyl bond contains a significant amount of ^{16}O (15%) while the peroxo bond mainly contains ^{18}O (97%) (**Figure 6**). The uranyl bond well integrates oxygen ^{18}O coming from the labelled water ($H_2{}^{18}O$ + $H_2{}^{18}O_2$ media), but also ^{16}O. The latter certainly comes from the solid and reflects an oxidation mechanism at the surface of the pellet. Indeed, the hypothesis of an initial release of the U^{4+} ion from the surface into the solution, followed by oxidation in the solution ($H_2{}^{18}O$ + $H_2{}^{18}O_2$ system), would have led to an ^{18}O enrichment close to 100%. Furthermore, $^{16}O_2$ coming from the air is 5 times less concentrated than $H_2{}^{18}O_2$ and its kinetic oxidation constant is 200 times lower [49], which does not support its participation in the uranium oxidation process.

With regard to the surface oxidation process in the presence of H_2O_2, it is generally described in two stages, with the formation of U(V) first, followed by the formation of the uranyl ion. A plausible mechanism proposed by Ekeroth and Jonsson [50] for the reaction between UO_2 and H_2O_2 is a primary slow one-electron transfer stage producing U(V) and OH° radicals according to the following reaction:

$$UO_2 + H_2O_2 \rightarrow UO_2^{+}{}_{surf} + OH° + OH^- \quad (7)$$

Which becomes by taking into account the isotopy of the studied system:

$$U^{16}O_2 + H_2{}^{18}O_2 \rightarrow U^{16}O_2{}^{+}{}_{surf} + {}^{18}OH° + {}^{18}OH^- \quad (8)$$

According to such a process, the formation of U(V) from H_2O_2 would not necessarily involve the incorporation of oxygen atoms into the fluorite structure. The formation of the uranyl ion can then be written [50]:

$$U^{16}O_2{}^{+}{}_{surf} + U^{16}O_2{}^{+}{}_{surf} \rightarrow U^{16}O_2{}^{2+}{}_{surf} + U^{16}O_2 \quad (9)$$

As the $^{18}OH°$ radicals formed, they can contribute to catalytic decomposition of H_2O_2 according to the following mechanism [51-53]:

$$H_2{}^{18}O_2 + M \rightarrow {}^{18}OH^- + {}^{18}OH°{}_{ads} + \mathbf{M^+} \quad (10)$$

$$^{18}OH°_{ads} + H_2{}^{18}O_2 \rightarrow H^{18}O_2° + H_2{}^{18}O \quad (11)$$

$$\mathbf{M^+} + H^{18}O_2° \rightarrow H^+ + {}^{18}O_2 + M \quad (12)$$

$$2\ H_2{}^{18}O_2 \rightarrow {}^{18}O_2 + 2\ H_2{}^{18}O \quad (13)$$

They can even oxidize the UO_2 surface. The relative contribution of these two processes (catalytic decomposition versus oxidation) depends in particular on the amount of OH° radicals scavenged by hydrogen peroxide [52]. Sunder [54] has proposed an interaction process between OH° and the surface

493 involving the incorporation of oxygen atoms into the fluorite structure. OH° radicals, produced during
494 the first oxidation step with H_2O_2 are smaller in size than the H_2O_2 molecule and can also oxidize the
495 surface. The UO_2 surface can incorporate oxygen atoms in an interstitial position according to the
496 following process [54]:

497 $$U(IV) + {}^{18}OH° \rightarrow H^+ + {}^{18}O_i^{2-} + U(V) \quad (14)$$

498 The interstitial ^{18}O oxygen atom can therefore also contribute to the formation of $UO_2^{+}{}_{surf}$ and $UO_2^{2+}{}_{surf}$
499 ions. More recently, studies on the interaction between water plasma and a UO_2 surface mention the
500 incorporation of oxygen atoms into the fluorite structure, resulting in a decrease of the U4f/O1s
501 surface area ratio measured by XPS [55]. Thus, the formation of the uranyl ion in the presence of $H_2{}^{18}O_2$
502 alone ($H_2{}^{18}O$ + $H_2{}^{18}O_2$ media), with both ^{18}O and ^{16}O isotopic contributions, is fully compatible with an
503 oxidation mechanism involving both electronic transfer and incorporation of interstitial oxygen from
504 the solution.

505 Therefore, it is interesting to discuss the isotopy of the uranyl bond for the alpha and gamma
506 irradiation experiments. For the gamma irradiation experiment, the uranyl bond is highly enriched up
507 to 95% in ^{18}O. The primary yields of OH° radicals for gamma radiation (low LET radiation) are high [35]
508 and these highly reactive species can rapidly interact with the UO_2 surface. The high reactivity of these
509 $^{18}OH°$ radicals produced by radiolysis of labelled water ($H_2{}^{18}O$) would lead to a massive incorporation
510 of ^{18}O at the surface and explain the low ^{16}O content of the uranyl ion. On the other hand, under alpha
511 irradiation, H_2O_2 peroxide remains a major product of water radiolysis and the primary production of
512 OH° radicals is 10 times lower than under gamma irradiation. Furthermore, the ^{18}O enrichments
513 obtained for the uranyl bond for the reference experiment with simple addition of $H_2{}^{18}O_2$ and for the
514 experiment under alpha irradiation with ^{18}O labelled water are very similar (figure 6). This observation
515 clearly argues for a predominant role of $H_2{}^{18}O_2$, especially after the beam has been cut. It is then
516 consistent to find the two isotopes (^{18}O and ^{16}O) of oxygen in the uranyl bond if processes involving
517 both electronic transfer and surface incorporation occur simultaneously under alpha irradiation.

518 It should be noted that under alpha irradiation and before the beam is cut off, the ^{18}O enrichment in
519 the uranyl bond is lower and the ^{16}O content is higher than after the beam is cut. This point may reflect
520 an increased mobility of oxygen atoms (^{16}O) in the solid due to the continuous creation of defects, but
521 will require additional development in the future. Another hypothesis is that the high local content of
522 hydrogen peroxide in the first seventy microns under alpha irradiation induces strong scavenging of
523 $^{18}OH°$ radicals.

524

5. Conclusion

An original experimental approach combining Raman spectroscopy to the use of $H_2{}^{18}O$ labelled water was developed to better understand the oxidizing dissolution of UO_2 and studtite precipitation mechanisms under alpha radiolysis of water. Two static leaching experiments were performed: the first involved the alteration of a UO_2 pellet under alpha radiolysis in the presence of ^{18}O-labelled water with in-situ Raman monitoring of the altered layer, and the second one involved the alteration of UO_2 in the presence of ^{18}O-labelled hydrogen peroxide. In these experiments, the precipitation of a studtite layer on the surface of the pellet was observed. It is clear that the bridging peroxo ligands in studtite originate from the peroxo species within the hydrogen peroxide molecule, which is itself produced by the radiolysis of water. Under alpha irradiation, the isotopic composition of the peroxide bond in studtite is essentially ^{18}O-^{18}O and originates from the $H_2{}^{18}O_2$ molecule formed by recombination of $^{18}OH°$ radicals in solution.

For the uranyl bond of the $UO_2{}^{2+}$ ions, the presence of both ^{16}O and ^{18}O isotopes is observed. This can be explained by allowing an oxidation process involving both a simple electron transfer by interaction with H_2O_2 and the incorporation of oxygen atoms coming from the solution into the fluorite structure due to oxidation by OH° radicals. The production of $^{18}OH°$ radicals, particularly by catalytic decomposition of hydrogen peroxide $H_2{}^{18}O_2$ on the surface of UO_2, remains a preferred route leading to the insertion of oxygen atoms into the material structure at the surface.

Moreover, these results are consistent with previous studies, this time carried out under gamma irradiation and in aerated conditions. The chemical relationship between the peroxide bond of H_2O_2 and the O-O bridging bond in studtite is also confirmed, as is the important role of OH° radicals in the insertion of oxygen atoms into the fluorite structure.

In the future, it will be useful to further investigate the role of atomic defects in the dynamics of isotopic exchange at the reaction interface. In this context, the use of a solid doped with ^{18}O, which allows the study of exchange dynamics within the solid under irradiation, would be relevant and is currently under extensive investigation.

Acknowledgments

The authors would like to express their gratitude to William Hate, Dominique Baux and Paul Sigot, members of the CEMHTI particles beams platform, for their technical support in this study. We are grateful to acknowledge Rachelle Omnée from CEMHTI and Stéphanie Szenknect from ICSM for their technical assistance. We would also like to thank Véronique Broudic from LMPA, Nicolas Clavier from ICSM and David Chaulin from CEMHTI for organizing the transport of the sample as well as Joseph Lautru from ICSM for the SEM analyses and Maxime Lanyi for his careful proofreading. Finally, the authors would like to thank the project Transport & Entreposage of the French Institut Tripartite CEA-EDF-Framatome for supporting this study.

CRediT

Aurelien Perrot: Writing – original draft, Methodology, Software, Formal analysis, Data curation, Investigation, Resources.

Aurelien Canizares: Methodology, Formal analysis, Data curation, Investigation, Resources, Writing – Review & Editing.

Sandrine Miro: Conceptualization, Validation, Formal analysis, Data curation, Investigation, Writing – original draft, Writing – Review & Editing, Visualisation, Supervision, Project administration, Funding acquisition.

Laurent Claparede: Conceptualization, Validation, Writing – Review & Editing, Visualisation, Supervision.

Renaud Podor: Methodology, Formal analysis, Data curation, Investigation, Resources, Writing – Review & Editing.

Thierry Sauvage: Conceptualization, Project administration, Writing – Review & Editing.

Sylvain Peuget: Writing – Review & Editing, Project administration, Funding acquisition.

Christophe Jegou: Conceptualization, Validation, Writing – original draft, Writing – Review & Editing, Visualization, Supervision, Project administration, Funding acquisition.

Nicolas Dacheux: Conceptualization, Validation, Writing – original draft, Writing – Review & Editing, Visualization, Supervision, Project administration, Funding acquisition.

References

[1] Burns, P.C., R.C. Ewing, and A. Navrotsky, *Nuclear fuel in a reactor accident.* Science, 2012. **335**(6073): p. 1184-1188 DOI: https://doi.org/10.1126/science.1211285.

[2] Ewing, R.C., *Long-term storage of spent nuclear fuel.* Nature Materials, 2015. **14**: p. 252-257 DOI: https://doi.org/10.1038/nmat4226.

[3] Hanson, B.D., et al., *Corrosion of commercial spent nuclear fuel. 1. Formation of studtite and metastudtite.* Radiochimica Acta, 2005. **93**(3): p. 159-168 DOI: https://doi.org/10.1524/ract.93.3.159.61613.

[4] Jégou, C., et al., *Oxidizing dissolution of spent MOX47 fuel subjected to water radiolysis: Solution chemistry and surface characterization by Raman spectroscopy.* Journal of Nuclear Materials, 2010. **399**(1): p. 68-80 DOI: https://doi.org/10.1016/j.jnucmat.2010.01.004.

[5] McNamara, B., et al., *Corrosion of commercial spent nuclear fuel. 2. Radiochemical analyses of metastudtite and leachates.* Radiochimica Acta, 2009. **93**: p. 169-175 DOI: https://doi.org/10.1524/ract.93.3.169.61615.

[6] Giménez, J., et al., *Cesium sorption on studtite ($UO_2O_2{\cdot}4H_2O$).* Radiochimica Acta, 2010. **98**(8): p. 479-483 DOI: https://doi.org/10.1524/ract.2010.1742.

[7] Kubatko, K.A.H., et al., *Stability of Peroxide-Containing Uranyl Minerals.* Science, 2003. **302**(5648): p. 1191-1193 DOI: https://doi.org/10.1126/science.1090259.

[8] Clarens, F., et al., *The oxidative dissolution of unirradiated UO_2 by hydrogen peroxide as a function of pH.* Journal of Nuclear Materials, 2005. **345**(2-3): p. 225-231 DOI: https://doi.org/10.1016/j.jnucmat.2005.06.002.

[9] Magnin, M., et al., *Oxidizing dissolution mechanism of an irradiated MOX fuel in underwater aerated conditions at slightly acidic pH.* Journal of Nuclear Materials, 2015. **462**: p. 230-241 DOI: https://doi.org/10.1016/j.jnucmat.2015.03.029.

[10] Forbes, T.Z., et al., *Alteration of dehydrated schoepite and soddyite to studtite, $[(UO_2)(O_2)(H_2O)_2](H_2O)_2$.* American Mineralogist, 2011. **96**(1): p. 202-206 DOI: https://doi.org/10.2138/am.2011.3517.

[11] Burns, P.B. and K.-A. Hughes, *Studtite, $[(UO_2)(O_2)(H_2O)_2](H_2O)_2$: The first structure of a peroxide mineral.* American Mineralogist, 2003. **88**(7): p. 1165-1168 DOI: https://doi.org/10.2138/am-2003-0725.

[12] Kim, J., et al., *Dissolution of studtite $[UO_2(O_2)(H_2O)_4]$ in various geochemical conditions.* Journal of Environmental Radioactivity, 2018. **189**(October 2017): p. 57-66 DOI: https://doi.org/10.1016/j.jenvrad.2018.01.010.

[13] Rey, A., et al., *Stability of uranium (VI) peroxide hydrates under ionizing radiation.* American Mineralogist, 2009. **94**(2-3): p. 229-235.

[14] Fairley, M., et al., *Stability of Solid Uranyl Peroxides under Irradiation.* Inorganic Chemistry, 2019. **58**(20): p. 14112-14119 DOI: https://doi.org/10.1021/acs.inorgchem.9b02132.

[15] Rey, A., et al., *Effect of temperature on studtite stability: Thermogravimetry and differential scanning calorimetry investigations.* Journal of Nuclear Materials, 2009. **385**(2): p. 467-473 DOI: https://doi.org/10.1016/j.jnucmat.2008.12.045.

[16] Thompson, N.B.A., et al., *The thermal decomposition of studtite: analysis of the amorphous phase.* Journal of Radioanalytical and Nuclear Chemistry, 2021. **327**(3): p. 1335-1347 DOI: https://doi.org/10.1007/s10967-021-07611-4.

[17] Sarrasin, L., et al., *Studtite Formation Assessed by Raman Spectroscopy and ^{18}O Isotopic Labeling during the Oxidative Dissolution of a MOX Fuel.* Journal of Physical Chemistry C, 2021. **125**(35): p. 19209-19218 DOI: https://doi.org/10.1021/acs.jpcc.1c04392.

[18] Canizarès, A., et al., *In situ Raman monitoring of materials under irradiation: Study of uranium dioxide alteration by water radiolysis.* Journal of Raman Spectroscopy, 2012. **43**(10): p. 1492-1497 DOI: https://doi.org/10.1002/jrs.4088.

[19] Guimbretière, G., et al., *Characterization of nuclear materials in extreme conditions: Raman spectroscopy approach.* IEEE Transactions on Nuclear Science, 2014. **61**(4): p. 2045-2051 DOI: https://doi.org/10.1109/TNS.2014.2311166.
[20] Martinez, J., et al., *An original precipitation route toward the preparation and the sintering of highly reactive uranium cerium dioxide powders.* Journal of Nuclear Materials, 2015. **462**: p. 173-181 DOI: https://doi.org/10.1016/j.jnucmat.2015.03.053.
[21] Ziegler, J.F., M.D. Ziegler, and J.P. Biersack, *SRIM - The stopping and range of ions in matter (2010).* Nuclear Instruments and Methods in Physics Research, Section B: Beam Interactions with Materials and Atoms, 2010. **268**(11-12): p. 1818-1823 DOI: https://doi.org/10.1016/j.nimb.2010.02.091.
[22] Soullard, J. and A. Alamo, *Etude du ralentissement des ions dans une cible diatomique.* Radiation Effects, 1978. **38**(3-4): p. 133-139 DOI: https://doi.org/10.1080/00337577808233221.
[23] Charlot, G., *Les méthodes de la chimie analityque: analyse quantitative minérale*. 5rd ed, Masson, Editor. 1966.
[24] Livneh, T. and E. Sterer, *Effect of pressure on the resonant multiphonon Raman scattering in UO_2.* Physical Review B - Condensed Matter and Materials Physics, 2006. **73**(8): p. 1-9 DOI: https://doi.org/10.1103/PhysRevB.73.085118.
[25] Allen, G.C., I.S. Butler, and T. Nguyen Anh, *Characterisation of uranium oxides by micro-Raman spectroscopy.* Journal of Nuclear Materials, 1987. **144**(1-2): p. 17-19 DOI: https://doi.org/10.1016/0022-3115(87)90274-1.
[26] Elorrieta, J.M., et al., *Temperature dependence of the Raman spectrum of UO_2.* Journal of Nuclear Materials, 2018. **503**: p. 191-194 DOI: https://doi.org/10.1016/j.jnucmat.2018.03.015.
[27] Gutierrez, G., et al., *Effect of ballistic damage in UO_2 samples under ion beam irradiations studied by in situ Raman spectroscopy.* Nuclear Instruments and Methods in Physics Research, Section B: Beam Interactions with Materials and Atoms, 2018. **434**(April): p. 45-50 DOI: https://doi.org/10.1016/j.nimb.2018.08.010.
[28] Jegou, C., et al., *Raman micro-spectroscopy of UOX and MOX spent nuclear fuel characterization and oxidation resistance of the high burn-up structure.* Journal of Nuclear Materials, 2015. **458**: p. 343-349 DOI: https://doi.org/10.1016/j.jnucmat.2014.12.072.
[29] Lv, J., et al., *Raman scattering from phonons and electronic excitations in UO_2 with different oxygen isotopes.* Journal of Raman Spectroscopy, 2015. **47**(3): p. 345-349 DOI: https://doi.org/10.1002/jrs.4785.
[30] He, H. and D. Shoesmith, *Raman spectroscopic studies of defect structures and phase transition in hyper-stoichiometric UO_{2+x}.* Physical Chemistry Chemical Physics, 2010. **12**(28): p. 8108-8117 DOI: https://doi.org/10.1039/b925495a.
[31] Lee, J., et al., *Raman spectroscopic study of the structural change of uranium–thorium-mixed oxides before and after oxidation.* Journal of Radioanalytical and Nuclear Chemistry, 2018. **316**(3): p. 1295-1300 DOI: https://doi.org/10.1007/s10967-018-5829-x.
[32] Guimbretière, G., et al., *In situ Raman monitoring of He^{2+} irradiation induced damage in a UO_2 ceramic.* Applied Physics Letters, 2013. **103**(4): p. 2-6 DOI: https://doi.org/10.1063/1.4816285.
[33] Corbel, C., et al., *Addition versus radiolytic production effects of hydrogen peroxide on aqueous corrosion of UO_2.* Journal of Nuclear Materials, 2006. **348**(1-2): p. 1-17 DOI: https://doi.org/10.1016/j.jnucmat.2005.05.009.
[34] Mohun, R., *Raman spectroscopy for the characterization of defective spent nuclear*. PhD thesis, Université Aix-Marseille, 2017. Available from: https://www.theses.fr/2017AIXM0288.pdf.
[35] Lucchini, J.-F., *Influence de la radiolyse a de l'eau sur l'alteration de la matrice UO_2 du combustible nucleaire usé*. PhD thesis, Universite Paris XI, 2001. Available from: https://inis.iaea.org/collection/NCLCollectionStore/_Public/46/131/46131462.pdf.

[36] Van der Lee, J., et al., *Module-oriented modeling of reactive transport with HYTEC.* Computers and Geosciences, 2003. **29**(3): p. 265-275 DOI: https://doi.org/10.1016/S0098-3004(03)00004-9.
[37] Giffaut, E., et al., *Andra thermodynamic database for performance assessment: ThermoChimie.* Applied Geochemistry, 2014. **49**: p. 225-236 DOI: http://dx.doi.org/10.1016/j.apgeochem.2014.05.007.
[38] Kurt, W., *On Studtite and Its Composition.* American Mineralogist, 1974. **59**(1-2): p. 166-171.
[39] Schlegel, M.L. and C. Jegou, *Uraninite alteration by H_2O_2 solutions and formation of secondary phases: An in situ microRaman spectroscopy and synchrotron X-ray diffraction study.* Journal of Nuclear Materials, 2022. **572**: p. 154056 DOI: https://doi.org/10.1016/j.jnucmat.2022.154056.
[40] Lu, G., A.J. Haes, and T.Z. Forbes, *Detection and identification of solids, surfaces, and solutions of uranium using vibrational spectroscopy.* Coordination Chemistry Reviews, 2018. **374**: p. 314-344 DOI: https://doi.org/10.1016/j.ccr.2018.07.010.
[41] Sunder, S. and H. Christensen, *Gamma Radiolysis of Water Solutions Relevant to the Nuclear Fuel Waste Management Program.* Nuclear Technology, 1993. **104**(3): p. 403-417 DOI: https://doi.org/10.13182/NT93-A34900.
[42] Hiroki, A., S.M. Pimblott, and J.A. LaVerne, *Hydrogen Peroxide Production in the Radiolysis of Water with High Radical Scavenger Concentrations.* J. Phys. Chem. A, 2002. **106**(40): p. 9352–9358 DOI: https://doi.org/10.1021/jp0207578.
[43] Jégou, C., et al., *Effect of external gamma irradiation on dissolution of the spent UO_2 fuel matrix.* Journal of Nuclear Materials, 2005. **341**(1): p. 62-82 DOI: https://doi.org/10.1016/j.jnucmat.2005.01.008.
[44] Joseph, J.M., et al., *A combined experimental and model analysis on the effect of pH and $O_{2(aq)}$ on γ-radiolytically produced H_2 and H_2O_2.* Radiation Physics and Chemistry, 2008. **77**(9): p. 1009-1020 DOI: https://doi.org/10.1016/j.radphyschem.2008.06.001.
[45] Iwamatsu, K., S. Sundin, and J.A. LaVerne, *Hydrogen peroxide kinetics in water radiolysis.* Radiation Physics and Chemistry, 2018. **145**: p. 207-212 DOI: https://doi.org/10.1016/j.radphyschem.2017.11.002.
[46] Bonales, L.J., et al., *Oxygen diffusion coefficient and characterization of leachant in UO2 corrosion studied by new methods.* Solid State Ionics, 2022. **380**(April): p. 1-8 DOI: https://doi.org/10.1016/j.ssi.2022.115922.
[47] Lonadier, F.D. and J.E. Boggs, *Isotope exchange studies on the uranium(VI) oxide hydrates and uranium peroxide.* J. Less-Common Met., 1963. **5**(2): p. 112-116 DOI: https://doi.org/10.1016/0022-5088(63)90003-1.
[48] Berger, P., *Etude du mécanisme de La dissolution par oxydoreduction chimique et electrochimique des bioxydes d'actinides (UO_2, NpO_2, PuO_2, AmO_2) en milieu aqueux acide*. PhD thesis, Paris VI, 1990. Available from: https://theses.fr/1988PA066073.
[49] Ekeroth, E., O. Roth, and M. Jonsson, *The relative impact of radiolysis products in radiation induced oxidative dissolution of UO_2.* Journal of Nuclear Materials, 2006. **355**(1-3): p. 38-46 DOI: https://doi.org/10.1016/j.jnucmat.2006.04.001.
[50] Ekeroth, E. and M. Jonsson, *Oxidation of UO_2 by radiolytic oxidants.* journal of Nuclear Materials, 2003. **322**(2-3): p. 242-248 DOI: https://doi.org/10.1016/j.jnucmat.2003.07.001.
[51] Jonsson, M., *An Overview of Interfacial Radiation Chemistry in Nuclear Technology.* Israel Journal of Chemistry, 2014. **54**(3): p. 292-301 DOI: https://doi.org/10.1002/ijch.201300119.
[52] Fidalgo, A.B., Y. Kumagai, and M. Jonsson, *The role of surface-bound hydroxyl radicals in the reaction between H_2O_2 and UO_2.* Journal of Coordination Chemistry, 2018. **71**(11-13): p. 1799-1807 DOI: https://doi.org/10.1080/00958972.2018.1466287.
[53] Maier, A.C., E.H. Iglebaek, and M. Jonsson, *Confirming the Formation of Hydroxyl Radicals in the Catalytic Decomposition of H_2O_2 on Metal Oxides Using Coumarin as a Probe.* Chemcatchem, 2019. **11**(22): p. 5435-5438 DOI: https://doi.org/10.1002/cctc.201901316.

[54] Sunder, S., et al., *Oxidation of UO_2 fuel by the products of gamma radiolysis of water.* Journal of Nuclear Materials, 1992. **190**: p. 78-86 DOI: https://doi.org/10.1016/0022-3115(92)90078-Y.

[55] El Jamal, G., et al., *Time-dependent surface modification of uranium oxides exposed to water plasma.* Dalton Transactions, 2021. **50**(14): p. 4796-4804 DOI: https://doi.org/10.1039/D1DT00486G.